Proportions of conical motifs: Optimal packing via the spherical image

Keith A. Seffen ●*

Advanced Structures Group, Civil Engineering Building, JJ Thomson Avenue, University of Cambridge, Cambridge CB3 0FA, United Kingdom

We present a scheme for calculating the shape of two well-known conical motifs: the d-Cone and the e-Cone. Each begins as a thin, flat disk, before buckling during loading into a deformed shape with distinctive, asymmetrical conical features and a localised apex. Various deformed equilibrium models rightly assume a *developable* shape, with a particular focus on determining how much of the disk detaches from how it is supported during buckling; they are, nevertheless, extensively curated analytically, and must confront (some, ingeniously) the question of singular, viz., infinite properties at the conical apex. In this study, we find an approximate description of shape that reveals the extent of detachment, from an analogous mobile vertex that packages optimally according to its constraints. To this end, we further develop the usage of *Gauss's Mapping* and the associated *spherical image*, which has been used previously, but only to confirm *known* properties of deformed shape. Despite the simplicity of our approach, remarkably good predictions are availed, perhaps because such problems of extreme deformation are geometrically (rather than equilibrium) dominated.

I. INTRODUCTION

We are familiar with making a cone, i.e., a conical surface, by removing a sector, e.g., using scissors and a paper card, and joining the exposed edges together smoothly; or by cutting a radial line and pulling the surfaces from either side to create an overlapping sector, which is easier to secure with, say, glue.

A larger sector angle, γ in Fig. 1(a), sets a steeper cone, Fig. 1(b), and vice versa. Bending the original disk into a cone requires effort set by the constitutive properties of the material and final shape, which is singly curved across straight-line generators radiating from the apex. Surface points sharing the same latitudinal circle have the same radius of surface curvature, r_1, which, from [1], is measured normal to the generator from the cone axis; see Figs. 1(c) and 1(d). When the circle radius is r, then

$$\tan \alpha = z/r, \quad \sin \alpha = r/r_1 \ \Rightarrow \ 1/r_1 = (\sin^2 \alpha / \cos \alpha)/z,$$
(1)

where $1/r_1$ is the curvature directly, and α is the conical semiangle relative to the horizontal.

Clearly, infinite curvature cannot occur at the apex where $z = 0$, even if it appears to be sharply defined. Moving towards the apex, maximal material strains rapidly increase according to the product of curvature and $t/2$, where t is the through-thickness: for example, a moderate semiangle of 30°

sets a limit of $z \approx 15t$ on the strain being smaller than 1%; any closer, $z < 15t$, and the strain is larger.

Furthermore, the elastic bending strain energy density is proportional to $(1/r_1)^2$ from the usual linear material constitution. The total energy stored is thus dominated by the apical region, whether or not plasticity features, which makes the deformation effort uncertain. However, a steeper cone has commensurately higher curvature at a given depth from the apex and is, clearly, "more" deformed: the increase in (nonlinear) bending strain energy density also outstrips the (linear) decrease in surface area—after sector removal—to which it applies.

Our story begins at this point and in Fig. 1(e), which shows, crudely, two circular figures traced on the top of a sphere of unit radius, or *unit sphere*. Each circle stems from mapping unit vectors normal to every conical generator moving around the apex on, say, a latitudinal circle in both cones in Fig. 1(a). Since every unit vector *along* a generator has the same orientation, the choice of latitudinal circle does not matter; and the size of each circular *spherical image* reflects the steepness (viz., deformation) of each cone.

The surface area of each spherical image, which is also highlighted, is equal to the angle (in radians) of the removed sector, where the unit radius of sphere avails consistent dimensions. This result, and the mapping technique, is the outcome of a "Remarkable Theorem" by Gauss (described in detail in [1]), whatever the outline shape of the image.

A simple proof for the circular variety first notes that the dashed perimeter length in the cut disk, $(2\pi - \gamma)R$, becomes the latitudinal circle of $2\pi r$. Hence, r/R, which is equal to $\cos \alpha$ in Fig. 1(c), is also equal to $1 - \gamma/2/\pi$, which sets $\gamma = 2\pi(1 - \cos \alpha)$. Auxiliary coordinates, x and θ, in Fig. 1(f) set the area of an elemental annulus on the unit sphere to be $(2\pi x)(1\delta\theta)$. Noting that $\sin \theta = (x/1)$ ("1" for unit radius), the integration is performed between limits of zero and α to
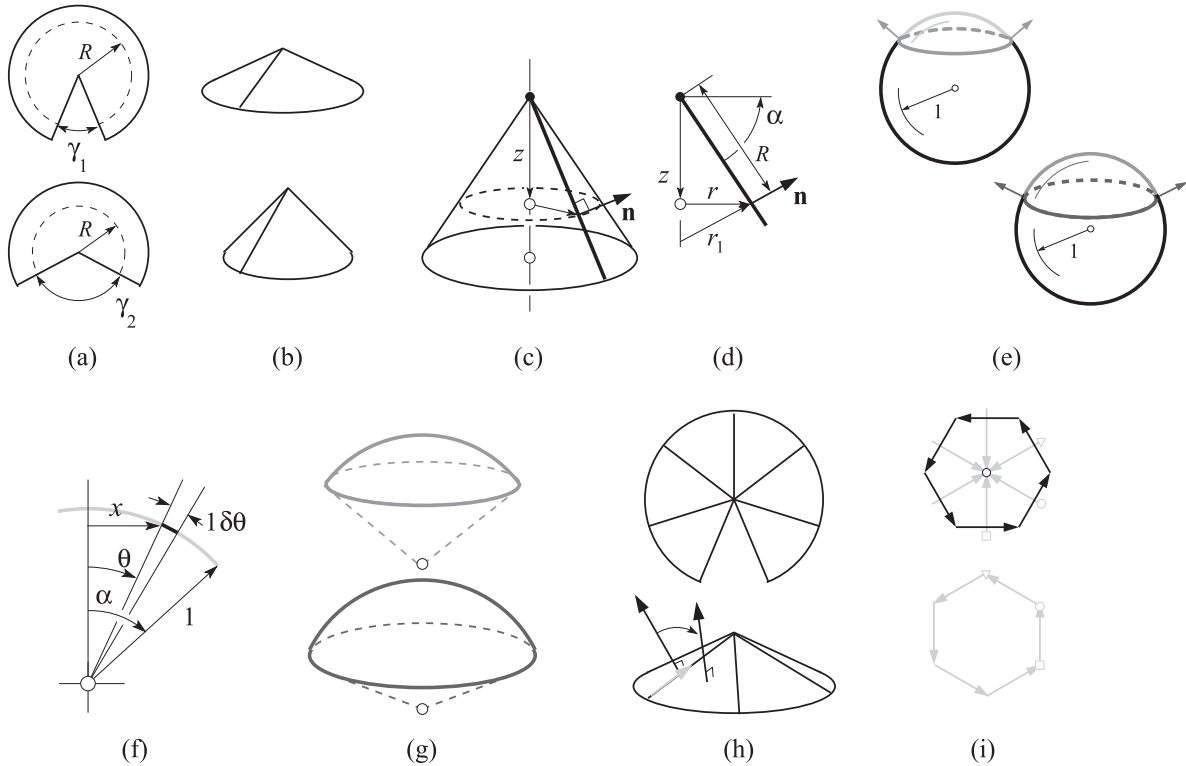
*kas14@cam.ac.uk

FIG. 1. Forming a cone from a flat disk, and associated geometrical concepts. (a) Two disks after removing differently sized sectors, where $\gamma_2 > \gamma_1$, now bent around and joined along the sector edges to form cones; (b) the γ_2 cone is steeper. (c) Typical straight-line generator (bold) from apex, with normal unit vector, **n**; (d) formal geometry of conical surface [assuming infinitesimal thickness, and cf. R from (a)]: r_1 is the radius of surface curvature and α is a semiangle. (e) Mapping of unit normals on a given latitudinal circle moving around the cone apex onto the surface of a unit sphere for both cones from (b), with corresponding circular spherical images: larger circle, steeper cone; smaller, shallower cone. (f) Auxiliary geometry for calculating the surface area of spherical images from (e), which form spherical "caps" in (g). Forming a cone instead by folding the disk along equispaced radial lines, (h), to give a faceted vertex approximation: the change in orientation of unit normals (black) to each facet is equivalent to the rotation angle between them, vectored along their connecting fold lines (light gray). (i) Top: plan-view of shallow spherical image from mapping the unit normals (black) from (h), with corresponding rotation vectors (light gray) superposed as a vector diagram centered on the apex node (center circle). The latter vectors can be added in sequence around the apex, bottom, to form the same spherical image, rotated by $90°$.

yield a spherical area equal to γ. Thus, the cone made from the larger sector angle, γ_2, initially has a larger spherical image than the one from γ_1, Fig. 1(g).

Let us now adjust these expectations in light of general images later, in three ways. The first deals with a *shallow* cone, made by removing a narrow sector. Its small spherical image sits atop the unit sphere, skirting the tangent plane at the pole; the difference, thus, between the true spherical area and that of the projection of the image onto this plane is negligible, and a much simpler calculation. The approximate area in the present circular case is $\pi\alpha^2$, which is no more than 1% different from the true value when α is less than $20°$, for example.

The second adjustment builds on the first. Consider forming each cone by *folding* along radial lines rather than by continuous curving, Fig. 1(h). We arrive at a discrete *vertex* with a finite number of flat facets approximating the cone shape. Each facet maps to a point on the unit sphere, which are joined together by *great arcs*, each of length equal in size to the abrupt rotation of normals about the fold lines, to give a *polygonal* spherical image [1]. A shallow vertex also gives way to a planar image but where the great arcs become

approximately straight and equal in scope to the rotation vectors along the fold lines. A *vector diagram* of the latter centered on the vertex but superposed onto the spherical image, Fig. 1(i), expresses equivalence in vector lengths and their relative inclinations but rotated altogether in plan-view by $90°$. There is, thus, no difference in using this set of rotation vectors to construct the same image by adding them nose-to-tail moving around the vertex, which is eminently simpler than the original mapping technique.

These two schemes were proposed by Farmer and Calladine [2], whose work inspires the first object of this article: the *developable cone*, or "d-Cone," in Fig. 2. They confirmed the already known proportions of d-Cone shape by reinterpreting Gauss's theorem in the context of small displacements, viz., rotations; they also record that a curved "crease" forms, rather than a point underneath the applied point force, which prescribes cylindrical displacements over part of the disk, rather than conical: we return to this point at the end.

Beforehand, and thirdly, the length of each rotation vector measures the local deformation in the fold line, whatever the intended analogy for continuous curving, which is a separate, diverse topic. For example, linear torsional springs are a
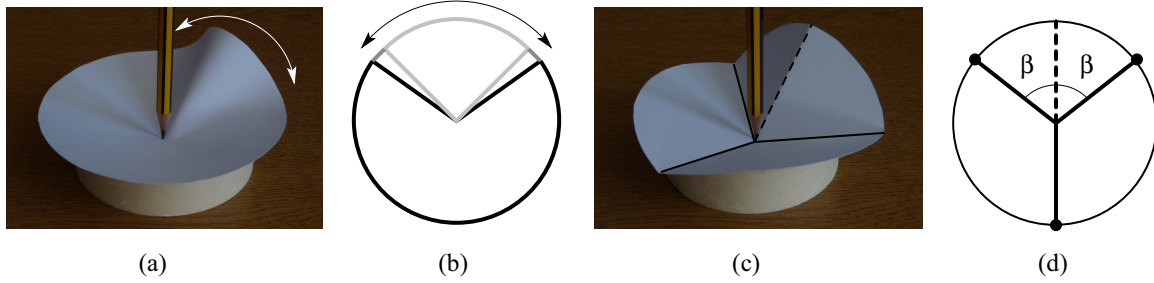
FIG. 2. A developable cone, or *d-Cone*. (a) Thin circular disk made of a paper card, simply supported close to its edge on a circular rim, indents conically under a central point force while buckling upwards and lifting off over around one-third of the circumference (white double arrow). (b) Deformation regimes: uniform conical indentation into page (black outline), everywhere supported on the rim; detached extent (double arrow) whose majority (light gray outlined sector) curves in the opposite sense to indenting, connected on both sides by narrow sectors managing the curvature transition. (c) Folded, faceted approximation of (a) via mountain fold line (dashed) and valley fold lines (solid). (d) Formal symmetrical planform geometry of (c): angular extent of detached area prescribed by two facet angles, β. Assuming the disk to be supported on its circumference initially, the three highlighted points are the eventual (and only) points of support during indentation (from [14]).

common proxy for elastic curving, whose effective stiffness is approximated by assuming the usual quadratic energetic form and comparing its expression to the continuum strain energy form undergoing the same global deformation [3,4]; but such stiffness ultimately depends on the width between fold lines, which approaches, again, a singular condition at the apex in the conical case (folding also creates a residual, or "rest" angle of folding, which further complicates the constitutive behavior).

Thinking purely, however, in deformation terms (and not in terms of stiffness or energy stored), the total length of the vectors, i.e., the *peripheral arc-length* of the image, rather than its areal size as originally surmised, quantifies the total deformation. Furthermore, the greater the number of facets, the higher the polygonal order and the smaller the individual rotation vectors become, before approaching a smooth outline in the limit of the continuous case; the areas of their corresponding spherical images should therefore converge for the same level of deformation.

In light of these geometrical ideas alone, our focus now turns to predicting the proportions of shape of a d-Cone and, later, its counterpart, the "e-Cone." Both of them form by lifting off, or detaching, from their supports during loading, where the detachment extent has been determined before using deformed equilibrium models that, nevertheless, must reconcile to the singular properties of any conical vertex—discussed in the next section; our analysis proposes to "circumvent" such matters.

II. THE D-CONE

When the center point of a rim-supported paper disk or any other very thin material is pushed inwards, the disk must shrink circumferentially. This action creates in-plane compression, which is meted by out-of-plane *buckling* initially because of the disk being thin.

Approximately two-thirds of the disk indents to a uniform cone impressing on the rim while the reminder gathers into a single, elevated wave, which has lifted off the rim in the opposite sense, altogether presenting as a developable cone, or d-Cone [5], in Fig. 2(a). The geometrical "shortening"

across the elevated wave is tantamount to removing a narrow sector of material, which expedites the remaining, indented conical shape. There is no actual deletion of material and no in-plane straining (neglecting any localized effects near the apex, including plastic), which creates a preference for conical bending about straight-line generators, hence the "developable" soubriquet according to Gauss's theorem.

The shape of the d-Cone is, thus, dominated by the indented and detached regions, and their approximate distribution is conveyed in Fig. 2(b). In-plane compression throughout foists a nonuniform distribution of conical curvature in the detached region, which is approximately proportional to the height of the detached disk above the rim. Moving from the indented region, the curvature must also change sign, which is accomplished in "transition zones" on the detached boundaries. Their corresponding sectors are also shown in Fig. 2(b), which distinguishes the remaining detached region to have opposite-sense conical curvature compared to the indented region, and in [5], e.g., they observe narrow transitional widths of around 20°.

In the face of these specificities, the subtended angular extent of the detached region is remarkably consistent (detailed momentarily) whatever the disk material (provided it is circular and supported the same), which has motivated research efforts over the past 25 years for an explanation. Furthermore, by unlocking the properties of a "regular" d-Cone shape in general, it is hoped to gain more insight into related problems expressing the same characteristic shape "motif" during extreme deformation in which holes or cuts do not appear, in problems of thin-walled buckling and crumpling.

Describing the displaced shape by means of curving across straight-line generators simplifies the kinematics somewhat, but their collective intersection near the apex depends on whether it forms as a single point or a short curved crease [2,5–7]. Either way, the introductory remarks about concentrated deformation persist, with the same implications for strain energy stored and/or stress, etc., in mechanical descriptions.

These "singularities" are typically circumvented in two ways: (i) Either physically, by introducing a small hole at the center, so that stresses or energy become concentrated but not
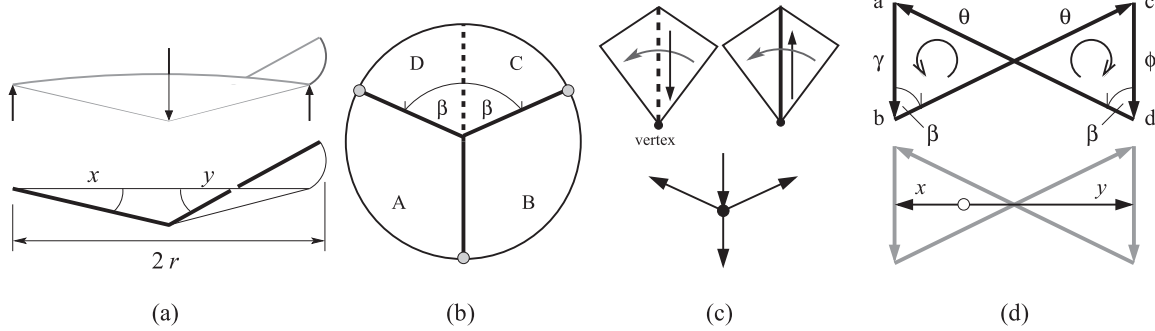
FIG. 3. d-Cone vertex kinematics. (a) Side-view rotations of central valley fold line, x, and mountain fold, y. (b) Facet labels, A, . . . , D, and three support points (filled gray circles). (c) Top: sign convention for fold-line rotation vectors: mountain fold lines point towards vertex; valley folds, away. Bottom: vector diagram of rotations for vertex in (b). (d) Top: corresponding spherical image from sequencing rotation vectors anticlockwise around the vertex: vectors ab, bc, . . . are relative rotations between facets A and B, B and C, . . . , denoted as γ, θ, and ϕ. Areas on both sides of the junction circulate in opposite senses and must be equal in size for a developable vertex. Bottom: location of horizontal plane (circle) and rotation vectors, x and y, from (a).

infinitely gathered—for any conical topography, including a "generally" creased disk: see, e.g., [7] and then [8]; or (ii) by solving analogous problems of thin strips deforming under constraint [9], which is justified separately in [7], who argue that the scaling laws for the geometrical dependency of the detached extent are not affected by the asymptotic variation of conical curvature at its apex.

Each of these approaches illuminates the d-Cone well, but the limits of operation have to be carefully curated for a robust equivalence of behavior. They are, nevertheless, consistent in their predictions of detached widths: in [7], they determine a subtended width of 138°, whereas in [5], they find 140°; their experiments indicate 127° and 130°, respectively, between two lift-off points on the rim. We now offer a different approach based on interpreting the spherical image of a d-Cone as a problem of *optimal packing* of its deformed state.

A "discrete" d-Cone is furnished in Fig. 2(c), where the symmetrical vertex is clearly similar in shape and proportions to the original continuous d-Cone. The width of the detached portion has been set *a priori* by the angular separation, 2β, of its exterior fold lines, which behave as transition zones of infinitesimal width, shown in plan-view before folding, in Fig. 2(d); the rotations across them then connect the upward folding facets of the detached portion to the downward folding, rim-supported facets. Two additional fold lines admit a viable out-of-plane motion: a central upwards *mountain* fold (shown as a dashed line), to be distinct from a third *valley* fold (drawn as a solid line), which bisects the indenting region.

The ability of this vertex in particular to fold *rigidly* as flat facets whatever the elastic response assumed for the fold lines conforms to theorems of Origami vertex folding from Makewa and Kawasaki [10], namely that mountains and valleys differ in their totals by two, i.e., one versus three, and that alternating facet angles sum to π radians. Motion can also proceed as far as being *flat-folded*, with all facets rotated relatively by π radians and coplanar.

Flat-folding is not an essential requirement when the limit of displacements is moderate in view of the accuracy of planar spherical images, and both theorems do not have to be strictly obeyed; the layout of fold lines must, nevertheless, sensibly

correlate with the continuum shape, and will therefore feature a mixture of mountain and valley fold lines, symmetrically arranged.

A schematic side view of the vertex in Fig. 3(a) directly shows the angle of inclination, x, of the center valley fold line relative to the original horizontal plane of disk, which sets the indented displacement to be $x.1$ (the dot denotes simple multiplication) for a disk radius equal to unity, whose (unit) significance is discussed at the end, and y for the mountain fold line moving upwards. Although initially supported simply everywhere at its edge, the folded disk rests on three points at the ends of the valley fold lines highlighted in Fig. 3(b).

For consistent notation, the rotations along mountain and valley lines are distinguished by vectors pointing towards or away from the vertex moving anticlockwise around it, which sets the corresponding vector diagram, Fig. 3(c), where the mountain fold-line rotation is ϕ, two rotations of θ for the side valleys, and γ for the central valley line: the facets are labeled A, . . . , D anticlockwise.

Placing the vectors nose-to-tail in the same order, we arrive at the planar approximation of the spherical image in Fig. 3(d). Since γ, for example, accords the rotation of facet A to B, its vector moves from "a" to "b" on the image, and so forth.

The "bow-tie" configuration divides the image into two areas, enclosed by vectors circulating in opposite senses, hence of opposite signs. Furthermore, because the vertex is formed without removing a sector, cf. Fig. 1, there can be no net area from Gauss's theorem [2], which stipulates equal areal portions.

This requirement therefore sets $\gamma = \phi$, and then $\phi = \theta \cos \beta$, i.e., there is one independent kinematic variable for this single degree-of-freedom system.

Rotation vectors corresponding to x and y are also appended to the image. Being normal to their respective fold-line rotations, γ and ϕ, places them horizontally on the image, straddling both vectors, γ to ϕ, and meeting them in their respective midpoints: they emanate from an origin point corresponding to the horizontal plane, as shown.

Calculating the central displacement via x and y relative to the rim support points, the following expressions from [14]
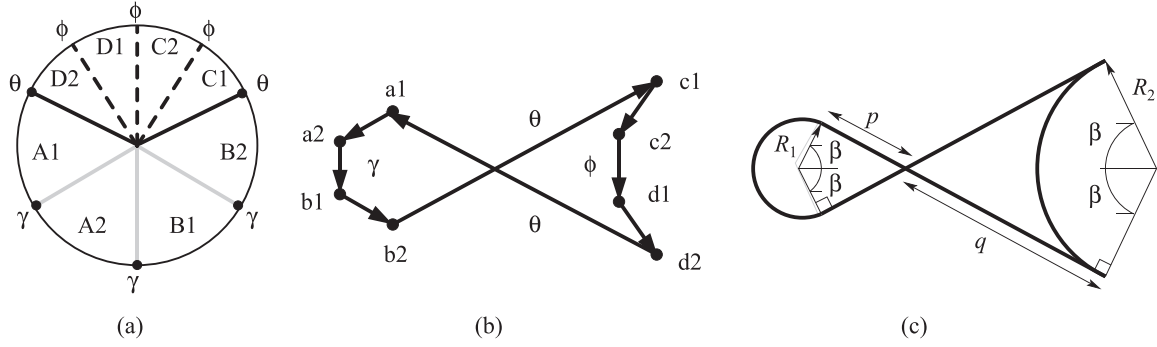
FIG. 4. More detailed d-Cone vertex. (a) Fold-line pattern (same legend as previous figure): transition zones remain as single fold lines, of rotations, θ. (b) Corresponding spherical image: fishlike, with head and tail about junction; both areas are equal in size for developability. (c) Continuum limit of (a) and (b), with infinitely many fold lines: R_1 and R_2 are auxiliary radii of circular arcs, for calculating equal areas of the head and tail.

are found:

$$x = (\phi/2)\tan(\beta/2), \;\; y = \phi\tan\beta - x. \tag{2}$$

We now surmise that the optimal packaged shape minimizes the folding deformation while maximizing the indentation, which loosely mimics a path of least action by the indenting force while respecting the support constraints. We therefore seek to minimize the ratio of the sum, $\phi + \gamma + 2\theta$, to x, which is defined to be Λ_d, where "d" denotes d-Cone:

$$\Lambda_d = \frac{2(\phi + \theta)}{x} = \frac{4\cos^2(\beta/2)}{\cos\beta\tan(\beta/2)} \tag{3}$$

after substituting for θ and x in terms of ϕ and β.

Differentiating with respect to β and setting equal to zero obliges us to solve

$$4\sin^4(\beta/2) - 5\sin^2(\beta/2) + 1 = 0. \tag{4}$$

The root according to minimal Λ_d is $\sin(\beta/2) = 1/2$, with a corresponding detached width, $2\beta = 120°$ (and $\Lambda_{d,\min} = 10.39$): $\gamma = \phi$, $\theta = 2\phi$, and $y/x = 5$ from Eq. (2): our predicted width is already close to practical observations (cf. $\approx 127°$).

To imitate the displaced shape better, more facets are created within the original scheme; see Fig. 4(a). One obvious template for intervening fold lines are the straight-line generators of the conical displacement field. Apart from the uniformly curved indented region, where generators are equispaced and furnish the same rotation, their distribution is nonuniform; furthermore, the concentrated curving in both narrow transition regions would suggest tightly spaced generators, viz., fold lines, which also accommodate a change in the direction of curving moving into the detached portion.

To avoid the need for extra parametrization necessary for such details at this stage, we assume that fold lines in the latter are also separately uniform and furnish equal rotations, γ: the indented region rotations are declared to be ϕ. For the same reason, the transition zones remain concentrated into single fold lines, across which the direction of facet articulation reverses instantaneously, from ϕ to γ towards the detached part. The consequences of having small, finite-width zones that, nevertheless, distribute the change in direction over more than one fold line are discussed later.

The corresponding spherical image is shown in Fig. 4(b), which is distinctly *piscine*, even though it is roughly constructed to express equal areas of the "head" and "tail" regions, $\theta \approx 5\phi$ ($\&\,5\gamma$), which highlights a more concentrated deformation in the narrow transition zones.

When the number of facets tends to infinity, the piecewise layouts of rotation vectors approach continuous curves (except for the transition zones). Figure 4(c), therefore, indicates three symmetrical peripheral features: a convex circular arc at the front, trailing back through intersecting straight lines to a reentrant arc in the rear. Each arc is defined by an auxiliary radius, R_1 and R_2, respectively, whose ratio determines the relative area between the head and tail, momentarily.

The front arc deals with the indented conical region and subtends $2\pi - 2\beta$; the straight lines have the usual length, θ, now split into convenient lengths p and q across their intersection—the junction of the head and tail. For the detached region, both ends of its reentrant arc connect to the θ lines at the same inclination, thereby subtending 2β, but where the path moving through both connections instantaneously reverses direction to form a *spinode* [12] [cf. the limit of Fig. 4(b)].

The area of the head region is denoted as A_1 and comprises two triangles of area $(1/2)R_1 p$ each, and a sector of area $(1/2)R_1^2(2\pi - 2\beta)$. For the tail, we subtract the sector area from the sum of two larger triangles: $A_2 = R_2 q - R_2^2\beta$. Noting that $\tan\beta$ is equal to p/R_1 and to q/R_2, the equal areas condition is set as

$$A_1 = A_2: \;\; R_1^2\tan\beta + R_1^2(\pi - \beta) = R_2^2\tan\beta - R_2^2\beta \;\; \Rightarrow$$

$$\rho^2 = \frac{\tan\beta - \beta + \pi}{\tan\beta - \beta}, \tag{5}$$

where $\rho = R_2/R_1$.

The peripheral arc-length, denoted as L_d, is equal to $R_1(2\pi - 2\beta) + 2(p + q) + R_2(2\beta)$. The rotation of the indenting generators about the support rim takes place at right angles to curving across them: on the spherical image, they are lines normal to the front arc, i.e., R_1, so the disk center must also indent by an amount equal to R_1 (recall: a disk of unit radius, initially).

The new "packing" ratio of total deformation to indentation displacement is now L_d/R_1. This is still denoted as Λ_d and
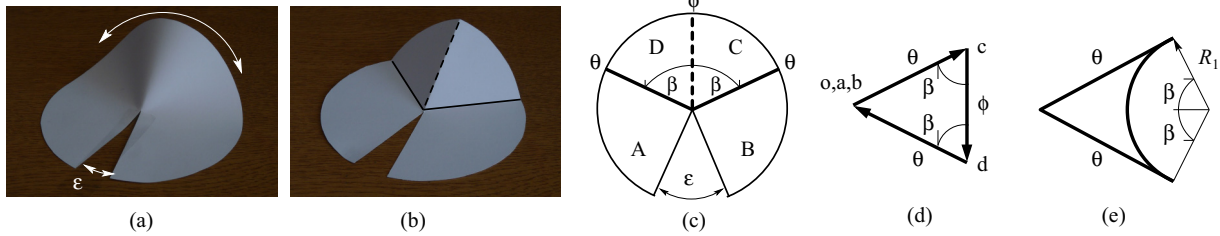
FIG. 5. Excess cone, or e-Cone. (a) Slit disk is opened up circumferentially by angle, ϵ, on a flat surface, causing the far side to buckle upward into an elevated cone (white double arrow). (b) Facet approximation via discrete folding with two valley fold lines (θ) and a single mountain fold (ϕ). Center point behaves as a vertex with excess angle, ϵ, above 2π. (c) Corresponding facet labels, for constructing vector diagram (same drawing convention as Fig. 4), hence a spherical image (d); continuum variant (e).

may be verified as the following function of β alone [after substituting for ρ from Eq. (5)]:

$$\Lambda_{\mathrm{d}} = 2 \left(\frac{(\tan\beta + \beta)(\tan\beta - \beta + \pi)^{1/2}}{(\tan\beta - \beta)^{1/2}} + \tan\beta - \beta + \pi \right). \tag{6}$$

Again, a minimum stems from differentiating Λ_{d} with respect to β and setting equal to zero, but without a solution in closed form. Instead, we plot the variation of Λ_{d} with β via MATLAB [11], and we arrive at Fig. 6(a), where $\Lambda_{\mathrm{d,min}} = 20.46$ when $2\beta = 106.3°$ (and $\rho = 2.95$): the detached width reduces marginally compared to $120°$ from earlier.

Compared to a practical width of around $130°$, this new result seems not as favorable. However, as noted, the actual transition regions subtend up to, and around, $20°$ each; we are, in fact, approaching the extent of the detached region ($\approx 90°$) outside of the transition regions which curves everywhere in the same sense as their corresponding fold lines in the spherical image. When finite-width transition zones are introduced later, albeit primitively described, the total detached width including these zones increases—along the lines of the observed result.

III. THE E-CONE

The *e-Cone* in Fig. 5(a) is formed by cutting a disk radially before opening up, as if to insert an additional sector perfectly, thereby creating an "excess" of angle subtended at the center
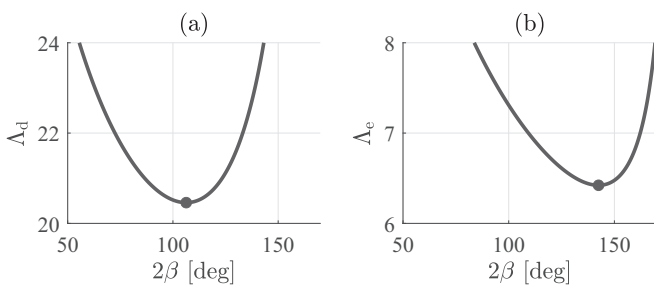

FIG. 6. Predictions of packaged shape as functions of width of detached regions, 2β. In both, Λ is the ratio of total deformation (viz., peripheral length of image) to the level of indentation displacement (d-Cone) or opening angle (e-Cone): (a) Eq. (6) for d-Cone; (b) Eq. (8) for e-Cone. Their respective minima (solid circles) occur when $2\beta = 106.3°$ and $142.5°$.

point. The disk is no longer supported on a rim but sits on the horizontal plane, forcing any displacements upward. Circumferential compression is now induced by increasing the opening angle, with part of the disk buckling above the horizontal plane, and symmetrically with respect to the opening sector. Again, a thin disk foists singly directed curving about radiating generator lines.

The e-Cone is not the antithesis of a d-Cone, rather, as the author purports in [14], it is the conjugate form of a *p-Cone* ("p" for "pyramidal"), which is simply either cone in Figs. 1(a) and 1(b): when the removed sector angle equals the opening angle of the e-Cone, these features superpose to our d-Cone precisely. Of course, the removed and opening sector angles can be different, as originally proposed in [13]; and the relative proportions of shape, expressed as a function of this difference and obtained from a modified spherical image in [14], correlate well with solving the more sophisticated *conical elastica* in [13].

Careful experiments also performed in [13] determine a consistent angular width of $180° \pm 5°$ of the region detached between a pair of radial lines on the flat surface. It is also apparent from the photographic data in Fig. 3 in [13] that approximately $120°$ of the elevated region (measured informally by the author) is curved in one sense, suggesting transition zones around $30°$ wide, which is slightly larger compared to a d-Cone. A finite-element analysis in [14] of the same experiment suggests a clearly discernible detached width of around $120°$ but without formally distinguishing, or measuring, the width of any transition zones. Nevertheless, we maintain zero-width transition zones, with a discussion at the end.

The simplest vertex approximation is given in Fig. 5(b), and the planform in Fig. 5(c) shows four facets, A, . . . , D, bounded by three fold lines straddling a prospective detached width of 2β, and the opening sector angle, ϵ. Facets A and B rotate in-plane to yield ϵ but only feature at the origin of the spherical image: C and D fold out-of-plane by a relative angle of ϕ, denoted as the rotation vector, cd, in Fig. 5(d); the valley rotations are, again, θ and thus as vectors ac and bd, which now close our spherical image.

From Gauss's theorem, the area of the image must equal ϵ, which is strictly negative when the rotation vectors in the image circulate in the opposite sense compared to the sign convention (but not essential for now). The level of folding deformation is simply $2\theta + \phi$, with $\cos\beta = \phi/2\theta$ from the
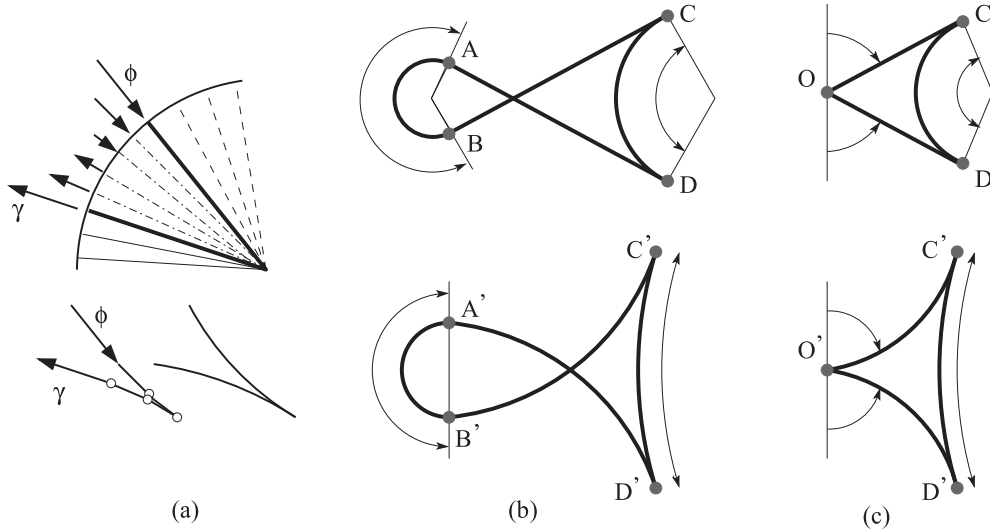
FIG. 7. (a) Effect of finite-width transition zone between elevated region (dashed fold lines) and the rest (e.g., d-Cone, solid fold lines). Rotations along the transition fold lines (dot-dashed) vary from one boundary rotation, ϕ, to the next, γ, which results in a discrete cusp; or a continuum cusp in the limit of infinitely many fold lines. (b) Top: original image from Fig. 4(c) for d-Cone: head, transition, and tail regions linked by AB, BC, CD, and DA, of nominal lengths. For finite-width transition zones, BC and DA become curved as B′C′ and D′A′, bottom, leading to a smaller arc-length, A′B′, corresponding to the indented region, thus larger detached width (including transition zones) overall. (c) Same adjustment process for e-Cone: top, original; bottom, incorporating finite-width transition zones as O′C′ and O′D′, giving a smaller cusp angle at O′ and hence a larger detached width.

image geometry, and the area of the image is $\phi\theta\sin\beta$, equal to ϵ.

For an equivalent statement of geometrical packing, we assume that the optimal shape is least folded for a given opening angle (or, indeed, opening arc-width equal to 1ϵ, the same, presuming a disk of unit radius, as usual). But since the opening angle is itself related in areal terms to the other rotations, we should normalize the area of the spherical image, say, to unity, which resets the original calculation: $1 = \phi\theta\sin\beta/\epsilon$, which is tantamount to rescaling the fold-line rotations to $\theta/\sqrt{\epsilon}$ and $\phi/\sqrt{\epsilon}$.

We therefore seek to minimize the peripheral length of the now rescaled image, which we define to be $\Lambda_{e,\min}$, i.e.,

$$\Lambda_e = 2(\theta/\sqrt{\epsilon}) + \phi/\sqrt{\epsilon} = \frac{\sqrt{2}(1 + \cos\beta)}{\sqrt{\sin\beta\cos\beta}} \quad (7)$$

after substituting for ϵ, etc. Differentiating with respect to β and setting equal to zero now obliges solving $2\cos\beta^2 + \cos\beta - 1 = 0$, which returns $\cos\beta = 1/2$ and a detached extent subtending $120°$ (and $\Lambda_{e,\min} = 3.22$).

Again, the image is refined by subdividing the detached region into many more equal facets, equally folded, while keeping the two valley folds. The limiting outcome for a uniformly conical shape is shown in Fig. 5(e), where the ϕ rotation vector is replaced by a circular arc of radius, R_1, connected to each θ line tangentially and subtending 2β, cf., Fig. 4(c).

Calculating the area enclosed, we find $2 \times (1/2)R_1\theta - (1/2)R_1^2(2\beta) = \epsilon$, which is rescaled to unity area, hence $(R_1/\sqrt{\epsilon})(\theta/\sqrt{\epsilon}) - (R_1/\sqrt{\epsilon})^2\beta = 1$. The edges of the spherical image are correspondingly rescaled by $1/\sqrt{\epsilon}$ and thus we

seek to minimize the new peripheral length:

$$\Lambda_e = 2(\theta/\sqrt{\epsilon}) + 2(R_1/\sqrt{\epsilon})2\beta = \frac{2(\tan\beta + \beta)}{\sqrt{\tan\beta - \beta}}. \quad (8)$$

Because there is no compact solution from setting $\partial\Lambda_e/\partial\beta = 0$, the variation of Λ_e with β is plotted in Fig. 6(b), which shows a minimum for $2\beta = 142.5°$ (and $\Lambda_{e,\min} = 6.42$).

IV. DISCUSSION

Our predictions of the detached extent in both conical motifs are plausible given our simplistic geometrical approach when compared to results from deformed equilibrium analysis: recall $138°$ for the d-Cone and $180°$ for the e-Cone; we predict, respectively, $106°$ and $143°$ (and $120°$ for both, from our simplest kinematical models).

We improved our "discrete" spherical images for both, to account for continuously shaped conical regions, but the transition zones always had infinitesimal width. If, instead, they had finite width, we would expect the total detached width, including the transition zones, to increase, potentially in line with known results and measurements.

For example, Fig. 7(a) shows a transition zone spanning a mountain fold-line rotation of ϕ and a valley rotation of γ over some width of disk, which is subdivided into facets. The rotations along their fold lines appeal to some continuous deformation by reducing in size before switching direction and then increasing.

These rotation vectors form a primitive cusp in the relevant part of the spherical image, which tend to continuous curves locally on either side of the cusp apex (when they were straight lines before): importantly, the curves do not have local

points of inflexion moving from ϕ to the apex, and then from the apex to γ. A new spherical image of the d-Cone, Fig. 7(b), therefore replaces the original straight θ lines, AD and BC, with concave curves, A'D' and B'C'.

This modification, however, introduces a subtended angle between their end points irrespective of the precise variation of fold-line rotation vectors in between, which must be "lost" elsewhere in the head and tail parts compared to original image, in order to accord a net sum of 2π for the exterior angles moving around the image; and, on satisfying equal head and tail areas from Gauss's theorem, it is most likely that *both* the original head and tail now subtend reduced angles. Now that the rim-supported portion is smaller, the detached width comprising the original, but now smaller, conical lifting region as well as the finite transition zones, must increase. The same argument also applies to the e-Cone; see Fig. 7(c).

This approach, of course, increases the parametrization required, which makes solving for optimally packaged shapes commensurately more difficult. Furthermore, as noted, the shape of the transition zones and the detached widths in general cannot be uniformly curved in practice because their bent shapes also sustain in-plane compressive forces.

Ultimately, any governing equation of coupled equilibrium expresses a kinematic variation in terms of a transverse displacement coordinate or the plate curvature itself, e.g., as in the conical elastica in [13]. Recasting such behavior in the context of the Gauss mapping may help to furnish a more accurate spherical and, hence, packaged result, and is part of ongoing study.

There are two other final comments. Farmer and Calladine [2] addressed the curved crease that forms underneath the point-load by discretizing the crease into a sequence of individual d-Cones sharing rotational properties along the crease, for a modest increase in the accuracy of the proportions of shape (recall that they assumed a nominal detached extent). We may do the same here, for a nontrivial amount of working.

Finally, our fold lines all have the same unit length: this will not be so in the case of other noncircular planform shapes, e.g., the two types of fold line of the square planform in [2] have a length ratio of $\sqrt{2}$, or when the load is no longer applied symmetrically, as trialled in [9]. The relative performance between fold-lines is therefore established per (their) unit length, in much the same way that moments and in-plane forces in continuum plates are unitary quantities; the indentation displacement is calculated appropriately.

In closing, employing Gauss's spherical image has brought a challenging problem of deformed equilibrium to heel in kinematical terms alone, with reasonable success. As an immediate extension of our approach, we shall shortly quantify the number of "truncated-cones" that form when a flat plate, intending to form as a d-Cone, suffers additional loading constraint, as studied recently in [15]. This study shows, prospectively, how straightforward our method can be extended to systems with a network of conical defects.

[1] C. R. Calladine, *Theory of Shell Structures* (Cambridge University Press, Cambridge, 1983).

[2] S. M. Farmer and C. R. Calladine, Geometry of 'developable cones', Int. J. Mech. Sci. **47**, 509 (2005).

[3] V. Brunck, F. Lechenault, A. Reid, and M. Adda-Bedia, Elastic theory of origami-based metamaterials, Phys. Rev. E **93**, 033005 (2016).

[4] Z. Y. Wei, Z. V. Guo, L. Dudte, H. Y. Liang, and L. Mahadevan, Geometric mechanics of periodic pleated origami, Phys. Rev. Lett. **110**, 215501 (2013).

[5] E. Cerda and L. Mahadevan, Conical surfaces and crescent singularities in crumpled sheets, Phys. Rev. Lett. **80**, 2358 (1998).

[6] S. Chaieb and F. Melo, Crescent singularities and stress focusing in a buckled sheet: Mechanics of developable cones, Phys. Rev. E **60**, 6091 (1999).

[7] T. Liang and T. A. Witten, Crescent singularities in crumpled sheets, Phys. Rev. E **71**, 016612 (2005).

[8] M. G. Walker, Mechanics of generically creased disks, Phys. Rev. E **101**, 043001 (2020).

[9] E. Cerda and L. Mahadevan, Confined developable elastic surfaces: Cylinders, cones and the elastica, Proc. R. Soc. London, A **461**, 671 (2005).

[10] K. Kasahara and T. Takaham, *Origami for the Connoisseur* (Japan Publications Trading Co., Chiyoda-Ku, Tokyo, Japan, 1998).

[11] The MathWorks Inc., MathWorks introduces release 2021b of MATLAB and Simulink, Natick, Massachusetts, USA, https://www.mathworks.com/company/newsroom/mathworks-introduces-release-2021b-of-matlab-and-simulink.html.

[12] E. W. Weisstein, Spinode: From MathWorld–A Wolfram Web Resource. https://mathworld.wolfram.com/Spinode.html

[13] E. Efrati, L. Pocivavsek, R. Meza, K. Y. Lee, and T. A. Witten, Confined disclinations: Exterior versus material constraints in developable thin elastic sheets, Phys. Rev. E **91**, 022404 (2015).

[14] K. A. Seffen, Fundamental conical defects: The d-cone, its e-cone, and its p-cone, Phys. Rev. E **94**, 013002 (2016).

[15] L. Stein-Montalvo, A. Guerra, K. Almeida, O. Kodio, D. P. Holmes, Wrinkling and developable cones in centrally confined sheets, Phys. Rev. E **108**, 035002 (2023).